

Analysis on Spatial Spectrum of Magnetic Flux Leakage Using Fourier Transform

Erlong Li¹, Yihua Kang¹, Jian Tang¹, Jianbo Wu², and Xizi Yan³

¹School of Mechanical Science and Engineering, Huazhong University of Science and Technology, Wuhan 430074, China

²School of Manufacturing Science and Engineering, Sichuan University, Chengdu 610065, China

³College of Engineering, Northeastern University, Boston, MA 02115 USA

As an efficient non-destructive testing method, magnetic flux leakage (MFL) has been widely used for damage detection in ferromagnetic materials. The magnetic dipole theory is a traditional method to calculate the magnetic leakage field. In this paper, the magnetic leakage field functions of a slot in a 2-D infinity plate are obtained using the magnetic dipole theory. Equations of the magnetic leakage field are converted into the convolution of two other functions. Spatial spectral equations of the MFL are developed according to the convolution theorem using the Fourier transform (FT) method. The results are analytical functions different from other numerical methods, such as the discrete FT and fast FT methods, and the calculation speed is fast. The results show that the y -component of the magnetic leakage field has 90° phase shift with the x -component. This result has clear physical significance compared with the traditional MFL equations using the magnetic dipole theory. Different spatial spectral curves for different defects are presented in this paper. Since there is a sinc function for the width value in the equation, the width value can be deduced from the first zero-crossing point in the spatial spectrum curves. A new method is proposed to determine the width value using the relationship $w = 1/f_s$, where f_s is the first zero cross point. Two specimens with different cracks are investigated, and the experimental results show this method can be used as an inverse MFL data interpretation technique.

Index Terms—Fourier transform (FT), magnetic dipole theory, magnetic flux leakage (MFL), spatial spectrum.

I. INTRODUCTION

THE magnetic flux leakage (MFL) is one of the most popular inspection methods in ferromagnetic material non-destructive testing (NDT) systems. It is widely used in the detection of steel pipe [1], [2], wire ropes [3], [4], oil tanks, and ferromagnetic plates. The basic theory of MFL is that the magnetic induction lines will escape from the ferromagnetic material under saturation magnetization conditions when there is a discontinuous volume, called the defect. Multiple magnetic sensors are used to measure the magnetic leakage field, such as halls, coils, and other magnetic sensors. The method can be used to estimate the width and depth values of defects by analyzing the magnetic leakage field signals. This technique has many excellent qualities, such as high speed, high precision, and no pollution [5].

Many efforts focus on developing models to explain the curves and characters of MFL signals. The two most popular methods to calculate the magnetic leakage field are the finite-element method [6], [7] and the magnetic dipole theory [8]. In addition, several parameters for the defects are obtained through the analysis of the waveform for the magnetic leakage field [9], [10]. The spectral information is another aspect to analyze the magnetic leakage field and the defect parameters, and it is important to calculate the spectral parameters of the MFL before designing the signal processing units. The spectrum in the MFL mostly consists of the temporal spectrum

and the spatial spectrum. The temporal spectrum can be used in pulse MFL and can improve the accuracy in NDT techniques [11]–[14], especially in calculating the depth value of a defect. In every testing point, the magnetic sensor has a temporal response curve, and the temporal spectrum is the Fourier transform (FT) result of the temporal response curve. The independent variable in this process is time, and the units of the temporal frequency are hertz. The spatial spectrum is another important aspect of the MFL and is distinct from the temporal spectrum. Spatial spectral functions of the MFL are obtained from the FT of the curves for changes in the magnetic leakage field component with the testing point. The spatial spectrum is the FT of the spatial domain, and the variable in the FT process is the length. The units of the spatial frequency are m^{-1} . In the dc MFL, when the testing speed is uniform, the temporal frequency is equal to the product of the speed and spatial frequency. Both the spatial and temporal spectra of the magnetic leakage have been calculated to date using the discrete FT (DFT), fast FT (FFT), short-time FT (STFT) [15]–[17], and other digital methods. However, the physical significance of the digital results is unclear. An analytical solution has many advantages compared with digital results.

In this paper, the x - and y -magnetic leakage field components from a traditional rectangular groove in a 2-D infinity plate are both expressed using the magnetic dipole theory, and the spatial spectra are developed using the FT method. Since the expression of H_x is a complex arctan function and H_y is a complex logarithmic function, it is difficult to calculate the FT results directly. A series of deformations is executed, and equations for H_x and H_y are transformed into the convolution of other functions. The FT

Manuscript received September 8, 2017; revised March 13, 2018; accepted May 30, 2018. Date of publication June 22, 2018; date of current version July 18, 2018. Corresponding author: E. Li (e-mail: lierlg720@126.com).

Color versions of one or more of the figures in this paper are available online at <http://ieeexplore.ieee.org>.

Digital Object Identifier 10.1109/TMAG.2018.2844220

0018-9464 © 2018 IEEE. Personal use is permitted, but republication/redistribution requires IEEE permission.
See http://www.ieee.org/publications_standards/publications/rights/index.html for more information.

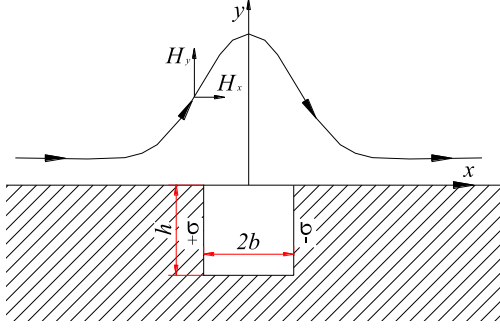


Fig. 1. Magnetic leakage field with the magnetic dipole model.

results are multiplied by the FT forms of other two functions according to the convolution theorem [18]. The FT results about the changing rate of magnetic leakage field are obtained using an integral transformation. This result is analytical, and the physical significance is discussed in this paper. The spatial spectral curves with different defects parameters are shown in this paper. A new method is proposed to estimate the width of the defect based on the spatial spectral curve, and experiments are conducted to verify this method. The analytical results are of great significance both in signal processing units and to evaluate the size of defects. This paper gives a new perspective of the MFL related to the spatial spectrum. Future work in this paper will focus on the linearization lift-off effect in the MFL and will propose other principles to design the MFL probes for the broad spatial spectrum.

II. FOURIER TRANSFORM OF THE MAGNETIC LEAKAGE FIELD

A. Calculated Magnetic Leakage Field Utilizing Magnetic Dipole Theory

In this section, a dipole model is developed to express the magnetic leakage field caused from a surface defect in the 2-D infinity plate shown in Fig. 1. The width and the depth of the defect are $2b$ and h , respectively. The magnetic charge densities on the flanks of the defect are assumed to be equivalent magnitudes of $+\sigma$ and $-\sigma$. The permeability of the specimen is μ_0 , and the detecting point is above the x -axis with a coordinate of (x, y) . The magnetic dipole model is shown in the following equations:

$$H_x(x, y) = \int_0^h (H_{1x} + H_{2x}) dy \quad (1)$$

$$H_y(x, y) = \int_0^h (H_{1y} + H_{2y}) dy \quad (2)$$

where $H_x(x, y)$ and $H_y(x, y)$ are the x - and y -components of the magnetic leakage field, respectively. H_{1x} and H_{2x} are the x -components of the magnetic leakage caused by the left and right flanks of the defect, and H_{1y} and H_{2y} are the y -components of the magnetic leakage caused by the left and right flank of the defect, respectively. The results of (1) and (2)

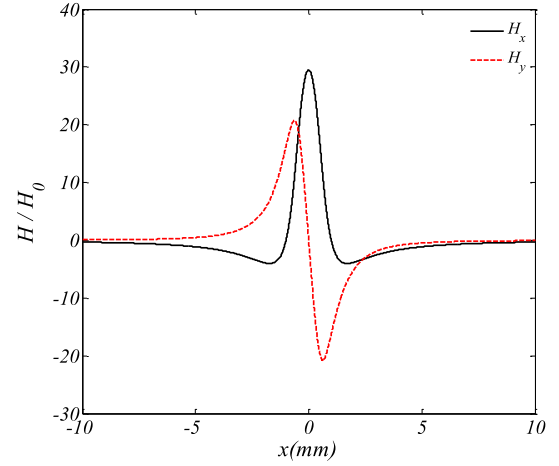


Fig. 2. Curves of H_x and H_y in the MFL.

are given in the following equations:

$$H_x(x, y) = \frac{H_0}{\pi} \left(\operatorname{atan} \frac{h(x+b)}{(x+b)^2 + y(y+h)} - \operatorname{atan} \frac{h(x-b)}{(x-b)^2 + y(y+h)} \right) \quad (3)$$

$$H_y(x, y) = \frac{H_0}{2\pi} \ln \frac{((x+b)^2 + (y+h)^2)((x-b)^2 + y^2)}{((x-b)^2 + (y+h)^2)((x+b)^2 + y^2)} \quad (4)$$

where H_0 is the magnetic field value inside the gap and is related to the magnetic charge density σ and the permeability of the specimen μ_0 . The magnetic field strength is a constant for the charge density and is equivalent on both flanks. When $2b = 1$ mm, $h = 1$ mm, and $y = 0.5$ mm, the curves of H_x and H_y are shown in Fig. 2. It is found from Fig. 2 that H_x is an odd function and H_y is an even function.

The magnetic sensor moves in the x -direction in the testing process, making x the independent variable. The FT method is applied to analyze the spatial spectrum information of the magnetic leakage field in the following equations:

$$H_x(\omega, y) = \int_{-\infty}^{+\infty} H_x(x, y) e^{-i\omega x} dx \quad (5)$$

$$H_y(\omega, y) = \int_{-\infty}^{+\infty} H_y(x, y) e^{-i\omega x} dx \quad (6)$$

where ω is the spatial frequency of the magnetic leakage field. It is difficult to calculate the results, which can be obtained using numerical methods based on the DFT and FFT or STFT. In Sections II-B–II-D, analytical solutions are obtained using the convolution theorem and FT method.

B. Fourier Transform of H_x in the Spatial Domain

It is difficult to directly obtain the result of the (5) and (6) because a series of transformations is necessary. First, the equation for H_x is divided by $y(y+h)$ for both the denominator and numerator, as shown in the following equation:

$$H_x(x, y) = \frac{H_0}{\pi} \left(\operatorname{atan} \frac{\frac{h(x+b)}{y(y+h)}}{1 + \frac{(x+b)^2}{y(y+h)}} - \operatorname{atan} \frac{\frac{h(x-b)}{y(y+h)}}{1 + \frac{(x-b)^2}{y(y+h)}} \right). \quad (7)$$

The result of (7) is shown in the following equation:

$$H_x(x, y) = \frac{H_0}{\pi} \left(\operatorname{atan} \frac{\frac{x+b}{y} - \frac{x+b}{y+h}}{1 + \frac{(x+b)(x+b)}{y(y+h)}} - \operatorname{atan} \frac{\frac{x-b}{y} - \frac{x-b}{y+h}}{1 + \frac{(x-b)(x-b)}{y(y+h)}} \right). \quad (8)$$

According to the trigonometric function quantification, the results of (8) are shown in the following equations:

$$H_x(x, y) = \frac{H_0}{\pi} \left(\operatorname{atan} \frac{x+b}{y} - \operatorname{atan} \frac{x+b}{y+h} - \operatorname{atan} \frac{x-b}{y} + \operatorname{atan} \frac{x-b}{y+h} \right) \quad (9)$$

$$H_x(x, y) = \frac{H_0}{\pi} \left(\operatorname{atan} \frac{x+b}{y} - \operatorname{atan} \frac{x-b}{y} - \frac{H_0}{\pi} \left(\operatorname{atan} \frac{x+b}{y+h} - \operatorname{atan} \frac{x-b}{y+h} \right) \right). \quad (10)$$

For convenience, $f(x, y)$ is introduced as (11), and (10) can be described as (12)

$$f(x, y) = \operatorname{atan} \frac{x+b}{y} - \operatorname{atan} \frac{x-b}{y} \quad (11)$$

$$H_x(x, y) = \frac{H_0}{\pi} f(x, y) - \frac{H_0}{\pi} f(x, y+h). \quad (12)$$

According to the integral formula, $f(x, y)$ has an integral form as shown in the following equation:

$$f(x, y) = \frac{1}{y} \int_{x-b}^{x+b} \frac{1}{1 + (\tau/y)^2} d\tau. \quad (13)$$

Another two functions are defined in the following equations:

$$g(x) = \frac{1}{1 + x^2} \quad (14)$$

$$p(x) = \begin{cases} 1 & (-b \leq x \leq b) \\ 0 & (|x| > 1). \end{cases} \quad (15)$$

The $f(x, y)$ can also be expressed the following equation:

$$f(x, y) = \frac{1}{y} \int_{-\infty}^{\infty} g\left(\frac{\tau}{y}\right) p(\tau - x) d\tau. \quad (16)$$

It is obvious that $p(x)$ is an even function with the relationship $p(x) = p(-x)$. Thus, (16) could be converted into as follows:

$$f(x, y) = \frac{1}{y} \int_{-\infty}^{\infty} g\left(\frac{\tau}{y}\right) p(x - \tau) d\tau = \frac{1}{y} g\left(\frac{x}{y}\right) * p(x). \quad (17)$$

According to the convolution theorem, a new function can be obtained as shown in the following equation:

$$F(\omega, y) = \frac{1}{y} \left(\mathcal{F} \left[g\left(\frac{x}{y}\right) \right] \cdot \mathcal{F}[p(x)] \right). \quad (18)$$

The FT of $g(x)$ and $p(x)$ is shown in the Appendix as $\mathcal{F}[g(x)]$ and $\mathcal{F}[p(x)]$. Thus, $F(\omega, y)$ can be expressed as

$$F(\omega, y) = 2b\pi e^{-|\omega y|} \operatorname{Sa}(\omega b) \quad (19)$$

where $\operatorname{Sa}(\omega b) = \sin(\omega b)/(\omega b)$. The FT solution of H_x is given by the following equation:

$$\begin{aligned} H_x(\omega, y) &= H_x(\omega, y) - H_x(\omega, y+h) \\ &= 2bH_0 e^{-|\omega y|} \operatorname{Sa}(\omega b) - 2bH_0 e^{-|\omega(y+h)|} \operatorname{Sa}(\omega b) \\ &= 2bH_0 e^{-|\omega y|} (1 - e^{-|\omega h|}) \operatorname{Sa}(\omega b). \end{aligned} \quad (20)$$

Results in (20) consist of three parts. The first part is a negative exponential function of the lift-off value y , the second part is a negative exponential function of defect depth value h , and the last part is a sinc function of the defect width b .

C. Fourier Transform of H_y in the Spatial Domain

The function of the y -component of the magnetic leakage field is shown in (4). In addition, a series of transformations should be conducted as follows. First, (4) could be separated into two parts as given in the following equation:

$$H_y(x, y) = \frac{H_0}{2\pi} \left[\ln \left(\frac{(x-b)^2 + y^2}{(x+b)^2 + y^2} \right) - \ln \left(\frac{(x-b)^2 + (y+h)^2}{(x+b)^2 + (y+h)^2} \right) \right]. \quad (21)$$

A new function $\varphi(x, y)$ is established in (22) and has a new form in (23)

$$\begin{aligned} \varphi(x, y) &= \ln \frac{(x-b)^2 + y^2}{(x+b)^2 + y^2} \\ &= \ln \left(\left(\frac{x-b}{y} \right)^2 + 1 \right) - \ln \left(\left(\frac{x+b}{y} \right)^2 + 1 \right) \end{aligned} \quad (22)$$

$$H_y(x, y) = \frac{H_0}{2\pi} [\varphi(x, y) - \varphi(x, y+h)]. \quad (23)$$

According to the integral formula in the Appendix, (22) has another form as

$$\begin{aligned} \varphi(x, y) &= - \int_{\tau=x-b}^{\tau=x+b} \frac{1}{1 + (\tau/y)^2} d\left(\frac{\tau}{y}\right) \\ &= - \frac{2}{y^2} \int_{x-b}^{x+b} \frac{\tau}{1 + (\tau/y)^2} d\tau \\ &= - \frac{2}{y^2} \int_{-\infty}^{\infty} \frac{\tau}{1 + (\tau/y)^2} p(\tau - x) d\tau \\ &= - \frac{2}{y^2} \int_{-\infty}^{\infty} \tau g\left(\frac{\tau}{y}\right) p(\tau - x) d\tau. \end{aligned} \quad (24)$$

Since $p(x)$ is an even function, it has the relationship $p(x) = p(-x)$. Therefore, (24) can be converted into the following equation:

$$\begin{aligned} \varphi(x, y) &= - \frac{2}{y^2} \int_{-\infty}^{\infty} \tau g\left(\frac{\tau}{y}\right) p(x - \tau) d\tau \\ &= - \frac{2}{y^2} \left[xg\left(\frac{x}{y}\right) \right] * p(x). \end{aligned} \quad (25)$$

This indicates that $\varphi(x, y)$ is the convolution of two other functions, such as $xg(x/y)$ and $p(x)$. According to the convolution theorem, a new function is established, as shown in the following equation:

$$\psi(\omega, y) = - \frac{2}{y^2} \mathcal{F} \left[xg\left(\frac{x}{y}\right) \right] \cdot \mathcal{F}[p(x)]. \quad (26)$$

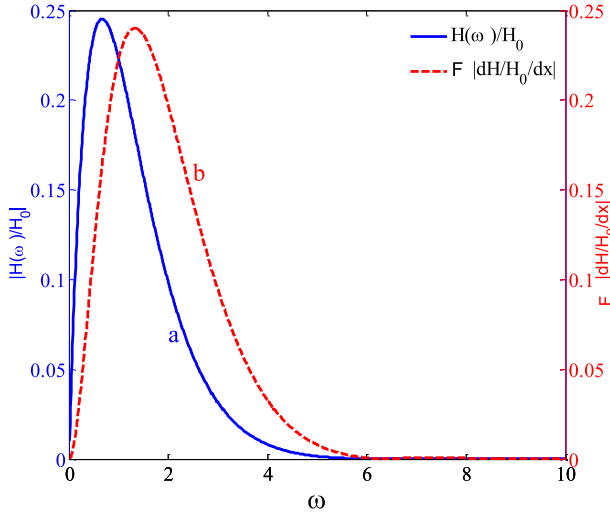


Fig. 3. Spatial amplitude frequency diagram of $H(2b = 1 \text{ mm}, h = 1 \text{ mm}, \text{ and } y = 1 \text{ mm})$.

The $\mathcal{F}[xg(x)]$ is shown in the Appendix, and the result of (26) is given by

$$\begin{aligned} \psi(\omega, y) &= -\frac{2}{y^2}(-i \operatorname{sgn}(\omega) \pi y^2 e^{-y|\omega|})(2b \operatorname{Sa}(\omega b)) \\ &= 4bi \operatorname{sgn}(\omega) \pi e^{-y|\omega|} \operatorname{Sa}(\omega b). \end{aligned} \quad (27)$$

According to (23), the FT of $H_y(x, y)$ can be described as follows:

$$\begin{aligned} H_y(\omega, y) &= \psi(\omega, y) - \psi(\omega, y + h) \\ &= 2bi H_0 \operatorname{sgn}(\omega) e^{-|\omega y|} \operatorname{Sa}(\omega b) \\ &\quad - 2bi H_0 \operatorname{sgn}(\omega) e^{-|\omega(y+h)|} \operatorname{Sa}(\omega b) \\ &= 2bi H_0 \operatorname{sgn}(\omega) e^{-|\omega y|} (1 - e^{-|\omega h|}) \operatorname{Sa}(\omega b). \end{aligned} \quad (28)$$

In comparison with (20), it can determine that the $H_y(\omega, y)$ has the same form as $H_x(\omega, y)$. The difference is a symbolic function of ω in $H_y(\omega, y)$. This is not a concern when the value of ω is less than zero in industrial applications and is only a concern when $\omega > 0$. At the same time, there is an imaginary number i in the proportional term of $H_y(\omega, y)$. This indicates that the phase of H_y has 90° shift in comparison with H_x . When the lift-off value y is larger than zero, the FT result of the magnetic leakage field is given in the following equation, if only the absolute value of the spectrum is considered:

$$\begin{aligned} |H_x(\omega, y)| &= |H_y(\omega, y)| \\ &= 2b H_0 e^{-\omega y} (1 - e^{-\omega h}) |\operatorname{Sa}(\omega b)| \quad (\omega > 0, y > 0). \end{aligned} \quad (29)$$

The curve from (29) is shown in Fig. 3 when the width is $2b = 1 \text{ mm}$, the depth is $h = 1 \text{ mm}$, and the lift-off value $y = 1 \text{ mm}$.

The results in Fig. 3 show that (29) is an increasing function initially, and it will decline after the vertex when the width of the defect is $2b = 1 \text{ mm}$, the depth is $h = 1 \text{ mm}$, and the lift-off value $y = 1 \text{ mm}$. Thus, a maximum value will appear in the curve of $|H(\omega)|$. In this situation, the center

frequency of H_x and H_y appears at the value $\omega = 0.67$. Several low-frequency components appear in the curve when $\omega < 0.67$ and are important parts of the magnetic leakage field, which could not be eliminated through the filter in the signal procession units. At the same time, some high-frequency components appear in the curve when $\omega > 0.67$, but the high-frequency amplitudes are less than 3.3% of the maximum value when $\omega > 4$, as seen from the amplitude frequency diagram.

D. Fourier Transform of dH_x/dx and dH_y/dx in the Spatial Domain

The changing rate of the magnetic leakage field is another important parameter for magnetic sensors such as coils in the MFL detecting system. In this section, the FT functions for the change rate of the x - and y -components for the magnetic leakage field are obtained. Two key conclusions are shown in the following equation based on (3) and (4):

$$\lim_{x \rightarrow \infty} H_x(x, y) = \lim_{x \rightarrow \infty} H_y(x, y) = 0. \quad (30)$$

The FT form of dH_x/dx is obtained from (31) and is shown in (32)

$$\begin{aligned} \mathcal{F}[dH_x/dx] &= \int_{-\infty}^{+\infty} \frac{dH_x}{dx} e^{-i\omega x} dx = \int_{-\infty}^{+\infty} e^{-i\omega x} dH_x \\ &= [H_x]_{x=-\infty}^{x=+\infty} + i\omega \int_{-\infty}^{+\infty} H_x e^{-i\omega x} dx \\ &= i\omega \mathcal{F}[H_x] \end{aligned} \quad (31)$$

$$\mathcal{F}[dH_x/dx] = 2i H_0 e^{-|\omega y|} (1 - e^{-|\omega h|}) \sin(\omega b). \quad (32)$$

The FT form of dH_y/dx is obtained from (33) and is shown in (34)

$$\begin{aligned} \mathcal{F}[dH_y/dx] &= \int_{-\infty}^{+\infty} \frac{dH_y}{dx} e^{-i\omega x} dx = \int_{-\infty}^{+\infty} e^{-i\omega x} dH_y \\ &= [H_y]_{x=-\infty}^{x=+\infty} + i\omega \int_{-\infty}^{+\infty} H_y e^{-i\omega x} dx \\ &= i\omega \mathcal{F}[H_y] \end{aligned} \quad (33)$$

$$\mathcal{F}[dH_y/dx] = -2 \operatorname{sgn}(\omega) H_0 e^{-|\omega y|} (1 - e^{-|\omega h|}) \sin(\omega b). \quad (34)$$

Since industrial applications are not concerned when the value of ω is less than zero, only the conditions when $\omega > 0$ are considered here. $\mathcal{F}[dH_x/dx]$ and $\mathcal{F}[dH_y/dx]$ are given in the following equation, if only the absolute value of the spectrum is concerned:

$$\begin{aligned} |\mathcal{F}[dH_x/dx]| &= |\mathcal{F}[dH_y/dx]| \\ &= 2H_0 e^{-\omega y} (1 - e^{-\omega h}) |\sin(\omega b)| \end{aligned} \quad (\omega > 0, y > 0). \quad (35)$$

The curves from (35) are shown in Fig. 4 when the width is $2b = 1 \text{ mm}$, the depth is $h = 1 \text{ mm}$, and the lift-off value $y = 1 \text{ mm}$.

The curve of Fig. 3(b) is similar to that of Fig. 3(a) but with a larger center frequency value that appears at $\omega = 1.33$. Fig. 4 shows the log spatial amplitude spectrum diagrams of the magnetic leakage field. The first zero-crossing points in Fig. 3 are shown in Fig. 4 as P1 and P2.

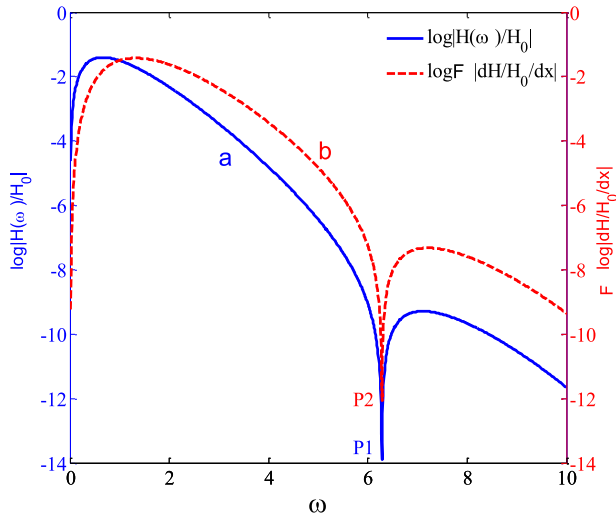


Fig. 4. Log spatial amplitude frequency diagram of H ($2b = 1$ mm, $h = 1$ mm, and $y = 1$ mm).

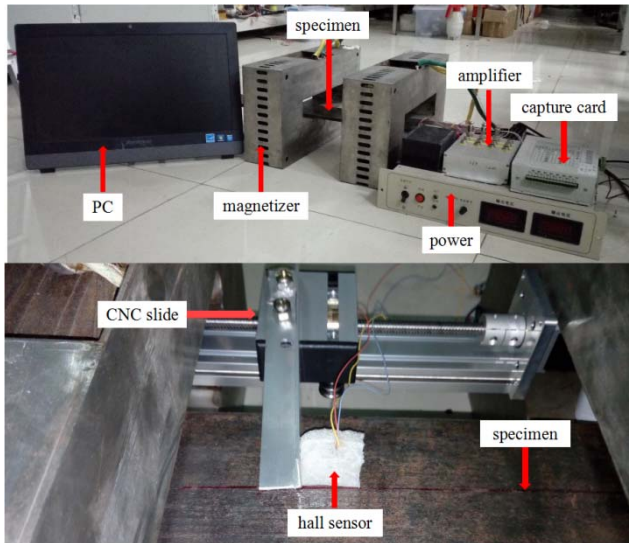


Fig. 5. MFL experimental platform for the plates.

III. EXPERIMENT

This section presents the experimental studies performed in the laboratory. The dc MFL is studied, and the signals are obtained when the sensor is moving across defects. The experimental apparatus consists of the specimens, a magnetizer, MFL detection unit, signal procession unit, power, data capture card, and the PC as shown in Fig. 5. The hall sensor is placed on a computer numerical control (CNC) slide, the number of turns for each magnetized coil is 300, and the dc current is 2 A. To eliminate the influence of the non-uniform magnetic field in the time domain, the current in the coil is uniform in the testing process. Thus, the magnetic leakage field will not change with time. The magnetic leakage field in each of the testing points will just change with the spatial domain.

Two steel plate samples, each containing four defects, are investigated using the dc MFL method, as shown in Fig. 6. The sizes of the defects are shown in Table I, where the

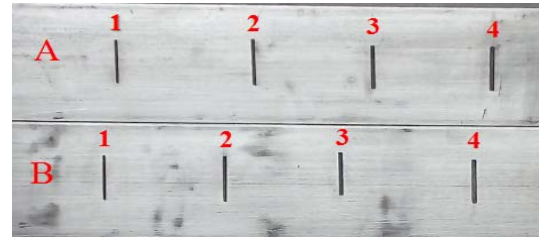


Fig. 6. Specimens and defects. (A) Specimen A, defects 1–4. (B) Specimen B, defects 1–4.

TABLE I
SIZE OF THE DEFECTS IN THE TWO SPECIMENS

Crack number	Size of defects, $2b$ (mm)* h (mm)	
	Sample name A	Sample name B
1	1.5*3	1.5*2
2	2*3	2*2
3	2.5*3	2.5*2
4	3*3	3*2

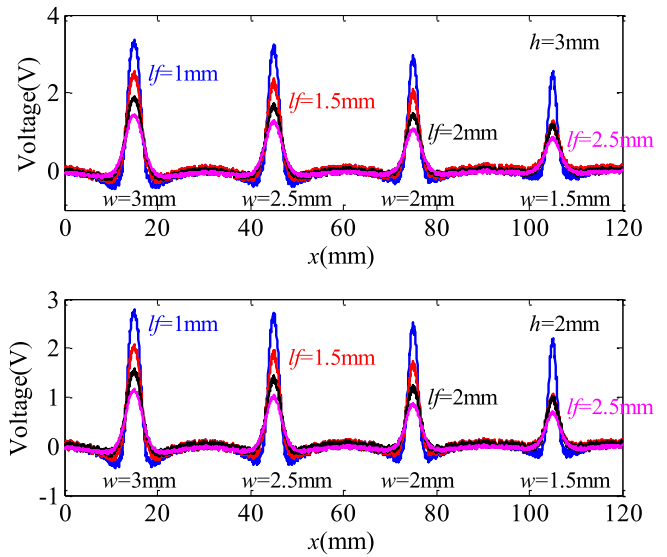


Fig. 7. MFL detection signals of the two specimens.

width is $2b$ and the depth is h with units of millimeters. In the industrial applications, the width value of defect is expressed by the parameter w , so the relationship between $2b$ and w is $2b = w$. The lengths are all equal to 30 mm, and the specimen thicknesses are all equal to 10 mm. The MFL signal is obtained from the hall sensor placed on a scanning station with a perpendicular scanning direction with respect to the defect after the signal amplifier unit. Lift-off values of the hall element are 1, 1.5, 2, and 2.5 mm, and the scanning speed of the CNC slide is 32.25 mm/s. A data capture card is applied to acquire the signal data after the signal amplification unit and has a sampling frequency of 50 kHz. Since the testing speed is uniform, the spatial sampling frequency can be calculated as the product with the scanning velocity with a result of 1550 mm^{-1} . The signals are shown in Fig. 7.

IV. RESULTS AND DISCUSSION

This paper provides an analytical equation of the spatial spectrum of the MFL, and its physical significance is discussed in this section. Different curves of the magnetic leakage field and spatial amplitude frequency diagrams are shown in this section. Since the spatial amplitude frequency diagram of the x -component has the same form as the y -component of the magnetic leakage field, only the x -component curves are considered. In addition, a new method is proposed to evaluate the width of the defect according to the spatial spectrum curve. The accuracy of this new method is verified through experiments.

A. Physical Significance of the Spatial Spectrum Equation

The spatial spectral equation for the MFL in this paper is shown in (29). Three terms in this equation are $e^{-\omega y}$, $1 - e^{-\omega h}$, and $2bSa(\omega b)$. These three items are named as the three functions $f_{\text{lift-off}}(y)$, $f_{\text{depth}}(h)$, and $f_{\text{width}}(2b)$ in the following equations:

$$f_{\text{lift-off}}(y) = e^{-\omega y} \quad (36)$$

$$f_{\text{depth}}(h) = 1 - e^{-\omega h} \quad (37)$$

$$f_{\text{width}}(2b) = 2b|Sa(\omega b)|. \quad (38)$$

Equation (29) can also be expressed as follows:

$$|H(\omega, y)| = H_0 f_{\text{lift-off}} \cdot f_{\text{depth}} \cdot f_{\text{width}}(\omega > 0, y > 0). \quad (39)$$

In (3) and (4), the lift-off value y , the depth h , and the width $2b$ are coupled in the same expression, and it is difficult to determine the influence of each item individually. A challenge in the MFL is the non-linear lift-off effect, which does not give a clear quantitative relationship between the lift-off value and the characteristic parameter of the MFL curves in Fig. 2 for different lift-off values. It is also difficult to obtain the quantitative relationship between the defect size and the curves in Fig. 2. However, in (39), the three factors of the defect in the MFL of the lift-off value, depth of the defect and width of defect are separated into three items in the spatial spectral domain and denoted as the lift-off function in (36), the depth function in (37), and the width function in (38).

As the lift-off value increases, the magnetic leakage field will decline, and the quantitative function can be described as a negative exponential function of the lift-off value y . The magnetic leakage field will be enhanced when the depth value increases. In the spatial spectral domain, the depth factor is expressed as a function given by $1 - e^{-\omega h}$. It can be seen from the results that both the lift-off value and the depth in the MFL have the same negative exponential relationship with each factor.

A slot is inscribed in the specimen as the defect in this paper. The geometric shape of defect can be described as a rect function with the independent variable as the width. Since the FT result of the rect function is an Sa function, there is an Sa function in the FT result of the MFL component in the spatial spectrum. The Sa function shows that there is a geometric discontinuity in the specimen. If the width of defect is small, the variable of the function in the geometric domain

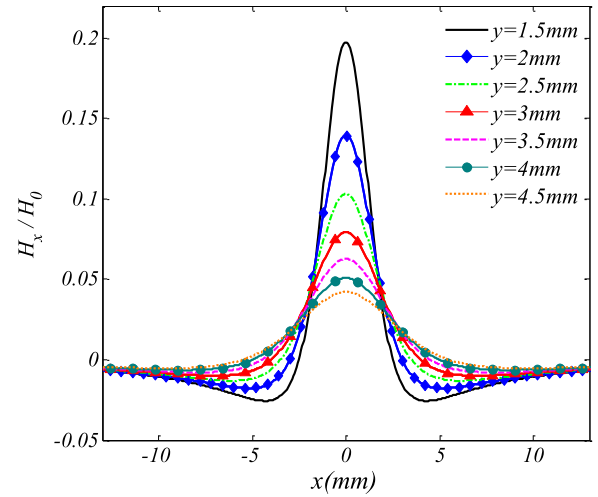


Fig. 8. Curves of H_x when $2b = 2$ mm, $h = 2$ mm, and y changes from 1.5 to 4.5 mm.

is small. However, the spatial frequency value will become bigger. In the width function, a clear relationship is revealed between the defect width and the spatial frequency.

The physical significance of the spatial spectrum of the MFL is discussed in this section. Comparing the traditional magnetic dipole function in (3) and (4), a clear physical significance is obtained, and the relationship between the magnetic leakage field and the testing parameter is clearer. Future works of this paper will be conducted to verify the lift-off value in the spatial spectrum and find other methods to invert the MFL signals in the spatial domain based on the analytical function in this section.

B. Spatial Amplitude Frequency Features With Different Testing Parameters Using Magnetic Dipole Theory

The curves of H_x are shown in Fig. 8 when the defect parameters are the width $2b$ of 2 mm, depth h of 2 mm, and when the lift-off value y changes from 1.5 to 4.5 mm using theoretical calculations. The log spatial amplitude frequency diagrams of H_x are shown in Fig. 9. The results show that the peak to peak value of the H_x will decline as the lift-off value increases, and the width of H_x will decline at the same time. The center frequency value will decline and the maximum value in the amplitude frequency diagram will decline as the lift-off value y increases. The conclusion is that the low-frequency components of H_x will increase and that the high-frequency components of H_x will reduce as the lift-off value increases. The MFL has been widely used in pipe NDT systems. The sensor was protected with a ferromagnetic piece between the pipe wall and the sensor, and the lift-off value is larger than 0.5 mm. In other situations, such as testing micro-cracks in bearing rings, the defect is smaller, and the lift-off value should be less than that in the pipe testing system. A result is that the spatial spectrum of the magnetic leakage field will be larger if the lift-off value is far less than 0.5 mm. In the future work, the lift-off value will be near zero to improve the testing capability of the MFL to detect micro-cracks. If the testing speed is kept at the same value, the sample rate of the system should be improved.

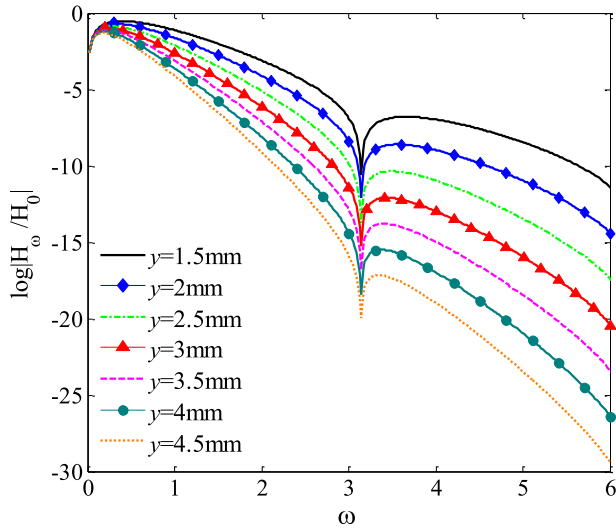


Fig. 9. Log spatial amplitude frequency diagram of H_x when $2b = 2$ mm, $h = 2$ mm, and y changes from 1.5 to 4.5 mm.

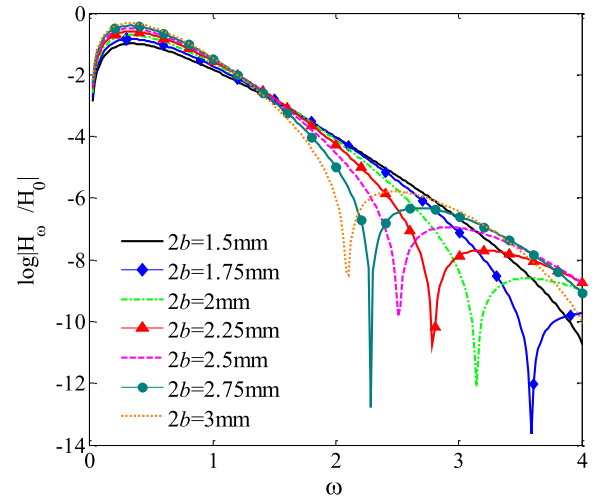


Fig. 11. Log Spatial amplitude frequency diagram of H_x when $h = 2$ mm, $y = 2$ mm, and $2b$ changes from 1.5 to 3 mm.

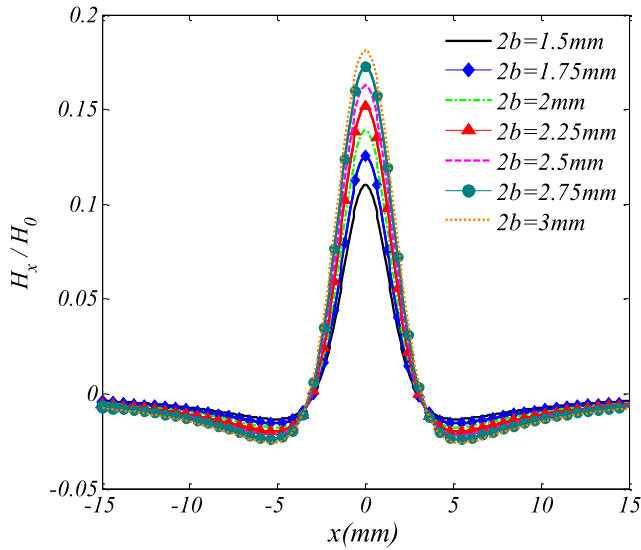


Fig. 10. Curves of H_x when $h = 2$ mm, $y = 2$ mm, and $2b$ changes from 1.5 to 3 mm.

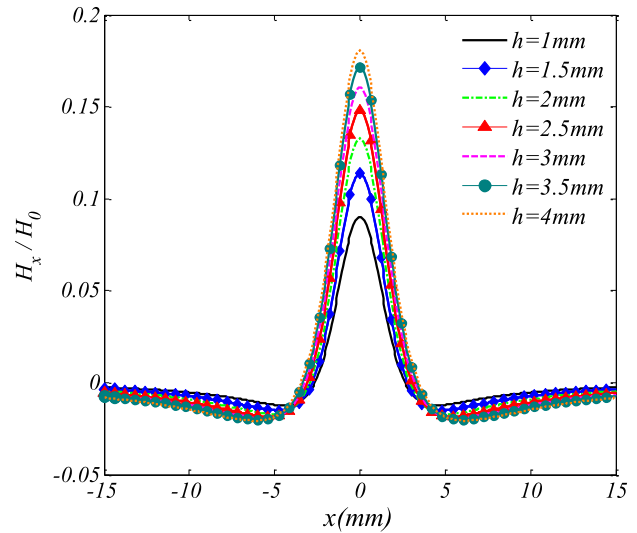


Fig. 12. Curves of H_x when $y = 2$ mm, $2b = 2$ mm, and h changes from 1 to 4 mm.

The testing signals of the MFL will be affected by the lift-off value, and it is difficult to find a parameter in the MFL curve that has a limited relationship with the lift-off value. The result is that a complex algorithm is necessary to calculate the defect parameters for different lift-off values. An independent feature point that has a limited relationship with lift-off values has many advantages in calculating the defect parameters. However, the first zero cross point in the spatial spectral curves has a limited relationship with the lift-off value. This means that the first zero cross point can be used to calculate the defect parameters.

Fig. 10 shows the H_x curves with different widths when the defect parameters meet the condition that the lift-off value y is 2 mm, the depth h is 2 mm, and the width $2b$ changes from 1.5 to 3 mm using theoretical calculations. Fig. 11 shows different log spatial spectral curves of H_x with different widths. The first zero cross points of the spatial spectrum curve

are different and will change with different widths, as shown in Fig. 11. This means that the first zero cross point can be used to calculate the width of the defects.

Fig. 12 shows the H_x curves for different depths when the defect parameters meet the conditions that the lift-off value l_f is 2 mm, the width $2b$ is 2 mm, and the depth h changes from 1 to 4 mm using theoretical calculations. Fig. 13 shows the log spatial spectral curves of H_x with different depths. The first zero cross points in the spatial spectral curves have a limited relationship with the depth, as shown in Fig. 13. The magnetic leakage fields will change with the depth of the defects, and there is not an independent feature point in the curve of the magnetic leakage field. It is also difficult to calculate the depth using the curves of the magnetic leakage field with a simple algorithm. However, the first zero cross point has a limited relationship with the depth. This means the first zero cross point in the spatial spectral curve has an excellent performance in evaluating the width of the defect. The judging principle has

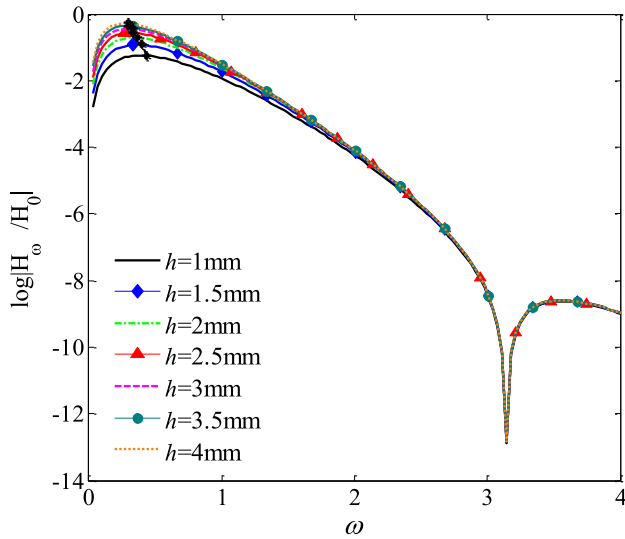


Fig. 13. Spatial amplitude frequency diagram of H_x when $y = 2$ mm, $2b = 2$ mm, and h changes from 1 to 4 mm.

a limited relationship with the lift-off value and the depth in the MFL. It is still a challenge to evaluate the depth of the defect from a future point in the curve of the spatial spectrum.

C. New Method to Evaluate the Defect Width Using the First Zero-Crossing Point in the Spatial Spectrum

The first zero cross point in the spatial spectral curve discussed in Section IV-C has a limited relationship with the lift-off value and depth. A new method is proposed to evaluate the defect width according to the first zero cross point. There is a width term in (38) for the spatial spectral function with the expression of $Sa(\omega b)$. The other terms, termed the lift-off function in (36) and the depth function in (37), are both larger than zero, so the first zero point in the spatial amplitude curve will appear when $\omega b = \pi$. A result is that the width could be implied from the first zero cross point in the spatial spectral curve according to the relationship of $b = \pi/\omega$.

In the experiment, the logarithmic spatial spectral diagram of H_x is of concern only for the results in Fig. 14. The first zero point in the spatial frequency diagram is replaced with the first minimum point in the logarithmic spectral diagram. The spatial frequency value is represented as f_s and has the relationship of $\omega = 2\pi f_s$. The logarithmic spatial spectral diagram of H_x when the defect depth is 2 mm and the widths are 1.5, 2, 2.5, and 3 mm is shown in Fig. 14(A). The logarithmic spatial spectral diagram of H_x when the defect depth is 3 mm and the widths are 1.5, 2, 2.5, and 3 mm is shown in Fig. 14(B).

The products of w and f_s are shown in Table II. It can be found that when $w = 3$ mm and $h = 2$ or 3 mm the products are equal to 0.807 and 0.822, respectively, and the errors are less than 20% compared with the theoretical result of $w \times f_s = 1$. In other situations, the error is less than 6% compared with theoretical results. Therefore, the first zero point in the amplitude frequency diagram of H_x will appear when $w \times f_s \approx 1$ according to theoretical analysis and experimental results when the defect depths are 2 and 3 mm and the width changes from 1.5 to 3 mm.

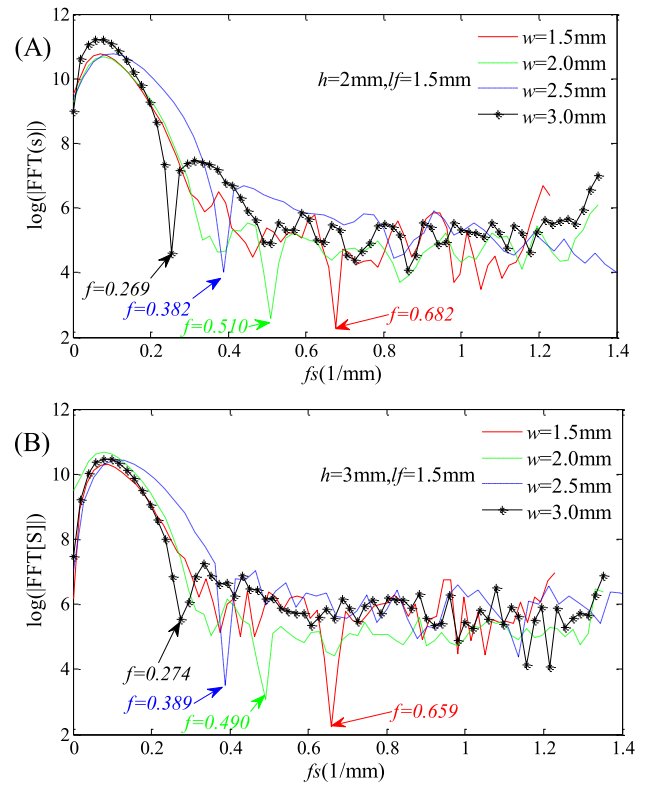


Fig. 14. Diagram of the logarithmic spatial spectrum through experiments. Testing results of (A) specimen A and (B) specimen B.

TABLE II
PRODUCT VALUES OF w AND f_s IN FIG. 14

lf (mm)	w (mm)	$w^* f_s$	
		$h=2$ mm	$h=3$ mm
1.5	1.5	1.023	0.9885
	2	1.02	0.98
	2.5	0.98	0.9725
	3	0.807	0.822

For other lift-off values, the relationships between the f_s and the lift-off value are shown in Fig. 15. Fig. 15(A) shows curves of $1/f_s$ and the width with different lift-off values obtained from the experiments in specimen A. Fig. 15(B) shows the experimental data from specimen B. The maximum testing errors all appear when the width is 3 mm. Different testing errors δ are all shown in Fig. 15.

The results in Fig. 15 show that the judging principle $w \times f_s = 1$ can be used for different lift-off values. The judging error is larger when the lift-off value is smaller when the width is 3 mm, as shown in Fig. 15(A) and (B). The functions of the magnetic leakage field in (3) and (4) are all obtained in the condition when the magnetic dipole charge density in the defect wall is uniform. These functions are not accurate if the magnetic dipole density is not uniform. The magnetic dipole density can be considered as uniform when the lift-off value is much larger than the width. The magnetic dipole density is no longer uniform when the lift-off value is in the same scale of width. The unevenness of the

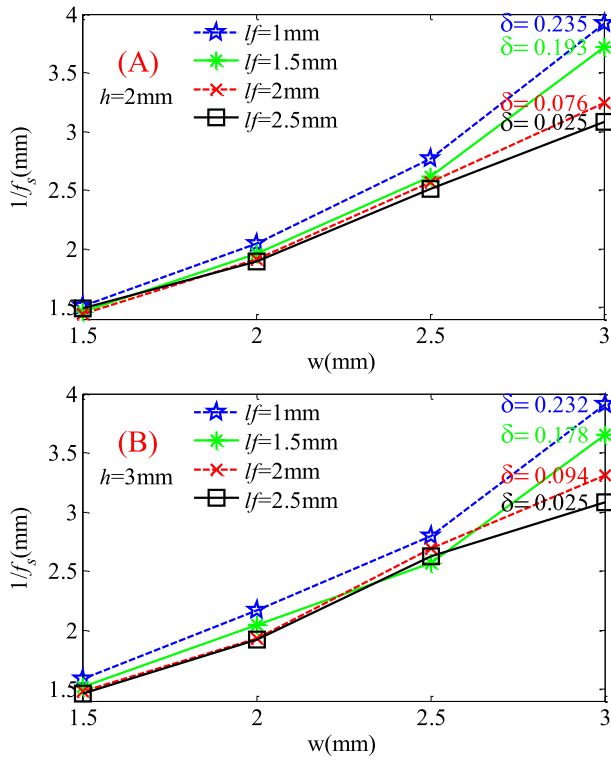


Fig. 15. Curves of w and f_s for different lift-off values. Results of (A) specimen A and (B) specimen B.

magnetic charge is more prominent when the lift-off value is smaller. Therefore, the maximum judging error will occur when the lift-off value is the least value ($lf = 1$ mm) and the width is the largest value ($w = 3$ mm). The judging errors in Fig. 15(A) and (B) when $lf = 3$ mm will be less when the lift-off values are larger. This means that it is difficult to evaluate defects with relatively large widths, especially when evaluating the width in corrosion defects using this method. Equation (3) and (4) are more accurate to describe the magnetic leakage field when the lift-off value is far larger than the width. However, it is difficult to detect cracks when the lift-off is too large based on the lift-off effect of the MFL. The lift-off function in (36) shows that the amplitude of the spatial spectrum will decline as the lift-off value increases, according to the negative exponential function $e^{-\omega y}$. The high-frequency components of the spatial spectrum in the MFL will decay rapidly when the lift-off value is much larger than the sizes of the defects. This means that the zero cross point is not obvious in the spatial spectral curves, and the results of this method are not stable. Thus, this method has difficulty when evaluating the defect width in very large lift-off values compared with the defect width. Another reason is that the MFL testing waveform is easily affected from changes in the lift-off value. The waveform of the MFL in such large lift-off values is easily affected by changes in the lift-off values. The high precision scanning sensor platform is necessary for high lift-off values. However, it is difficult to provide such a high precision scanning platform in industrial applications.

Natural defects have many different sizes and shapes, and it is difficult to evaluate the width of complex shaped cracks. The spatial spectral curve for small defects has more high-frequency components. This means the sampling

frequency should be larger than the detecting defects in specimens A and B. At the same time, the moving speed should be strictly consistent, and the lift-off value should not be changed. Testing errors will occur by changing the moving speed and the lift-off values in the testing process. This paper proposed a new method to evaluate the width of a slot etched in a plate. The testing sensor is a hall element and the length of defects is not considered. Sensors with sensitive lines are typically used to detect cracks with long length values. These sensors obtained more energy in the magnetic leakage field. The testing signal is the average component of the magnetic leakage field. Testing errors using this method will be larger when detecting cracks with curved shapes. All the influencing factors using the proposed method in (3) and (4) will introduce testing errors.

In industrial applications, it is important to calculate the width of the defect in the MFL detection system. There is not a clear quantitative relationship between the defect width and the key point in H_x and H_y curves in the MFL. However, in the spatial spectrum domain, a simple relationship between the width and the first zero cross point is revealed. The width could be approximately deduced from the relationship of $w = 1/f_s$, and f_s is the first zero cross point in the amplitude frequency diagram of the MFL signal obtained from the hall sensor. This paper proposed a new theoretical method to evaluate this approach.

V. CONCLUSION

In this paper, the analytical results of the FT solutions for the magnetic leakage field caused from a slot in a 2-D infinite plate are established, and the FT solutions for its change rate are obtained. Some conclusions are obtained as follows.

- 1) The spatial spectrum of the MFL is obtained first from the FT method. The results show that the y -component of magnetic leakage field has 90° phase shift compared with the x -component.
- 2) Distinct from the magnetic dipole function in the MFL, the lift-off function, depth function, and width function are separated into three items. The physical significance of the spatial spectral function is cleaner. This method gives a brief relationship between the testing parameters and the magnetic leakage field.
- 3) A new method is proposed to calculate the width of the defect according to the zero cross point in the spatial spectral curve from the relationship of $w = 1/f_s$, and the value of f_s is when the first zero cross point appears in the spatial amplitude frequency curve of the MFL signal. This method has a limited relationship with the lift-off value and depth.
- 4) This method has difficulty when evaluating defects with large widths since the magnetic dipole density is no longer uniform on the wall of the slot. It is also difficult to evaluate small defects since the testing error of the magnetic leakage field will become larger.

In this paper, the analytical spatial spectral function in the MFL is proposed. However, the function is based on the magnetic dipole theory, the magnetic charge density in the wall of the defect is not always uniform, and the results are not

always accurate. Thus, a new, more accurate function in the spatial spectrum should be researched in the future.

APPENDIX

Some integral formulae and FTs of functions are shown in this section [18]

$$\int \frac{1}{1+x^2} dx = \text{atanx} + c \quad (40)$$

$$\int \frac{1}{1+x} dx = \ln x + c \quad (41)$$

$$\mathcal{F}[g(x)] = \mathcal{F}\left[\frac{1}{1+x^2}\right] = \pi e^{-|\omega|} \quad (42)$$

$$\mathcal{F}[f(ax)] = \frac{1}{|a|} F\left(\frac{\omega}{a}\right) \quad (43)$$

$$\mathcal{F}[xf(x)] = i \frac{d}{d\omega} F(\omega). \quad (44)$$

Since the function $g(x/y)$ has the expression $g(x/y) = 1/[1+(x/y)^2]$, its FT is shown as

$$\mathcal{F}\left[g\left(\frac{x}{y}\right)\right] = \pi |y| G(y\omega) = \pi |y| e^{-|\omega y|}. \quad (45)$$

Since y is the lift-off value and is greater than zero, $|y| = y$, and the result is

$$\mathcal{F}\left[g\left(\frac{x}{y}\right)\right] = \pi |y| G(y\omega) = \pi y e^{-y|\omega|} \quad (46)$$

$$\mathcal{F}\left[xg\left(\frac{x}{y}\right)\right] = i \frac{d}{d\omega} \pi y e^{-y|\omega|} = -i \text{sgn}(\omega) \pi y^2 e^{-y|\omega|}. \quad (47)$$

The $p(x)$ is another key function in this paper, and its FT is shown as

$$\begin{aligned} \mathcal{F}[p(x)] &= \int_{-b}^b e^{-i\omega x} dx = \int_{-b}^b [\cos(\omega x) - i \sin(\omega x)] dx \\ &= \int_{-b}^b \cos(\omega x) dx = 2b \frac{\sin(\omega b)}{\omega b} = 2b \text{Sa}(\omega b). \end{aligned} \quad (48)$$

REFERENCES

- [1] Z. D. Wang, Y. Gu, and Y. S. Wang, "A review of three magnetic NDT technologies," *J. Magn., Magn. Mater.*, vol. 324, no. 4, pp. 382–388, 2012.
- [2] Y. Shi, C. Zhang, R. Li, M. Cai, and G. Jia, "Theory and application of magnetic flux leakage pipeline detection," *Sensors*, vol. 15, no. 12, pp. 31036–31055, 2015.
- [3] N. Sumyong, A. Pratepasen, and P. Kaewtrakulpong, "Influence of scanning velocity and gap distance on magnetic flux leakage measurement," *ECTI Trans. Elect. Eng., Electron. Commun.*, vol. 5, no. 1, pp. 118–122, 2007.
- [4] F. Xu, X. Wang, and H. Wu, "Inspection method of cable-stayed bridge using magnetic flux leakage detection: Principle, sensor design, and signal processing," *J. Mech. Sci. Technol.*, vol. 26, no. 3, pp. 661–669, 2012.
- [5] Y. Wang, "Testing of MFL for ferromagnetic materials," *J. Electron. Meas., Instrum.*, vol. 3, no. 3, p. 10, 2000.
- [6] F. I. Al-Naemi, J. P. Hall, and A. J. Moses, "FEM modelling techniques of magnetic flux leakage-type NDT for ferromagnetic plate inspections," *J. Magn., Magn. Mater.*, vol. 304, no. 2, pp. e790–e793, 2006.
- [7] F. Ji, C. Wang, S. Sun, and W. Wang, "Application of 3-D FEM in the simulation analysis for MFL signals," *Insight-Non-Destruct. Testing Condition Monit.*, vol. 51, no. 1, pp. 32–35, 2009.
- [8] J. Philip, C. B. Rao, T. Jayakumar, and B. Raj, "A new optical technique for detection of defects in ferromagnetic materials and components," *NDT & E Int.*, vol. 33, no. 5, pp. 289–295, 2000.
- [9] Y. Sun, C. B. Rao, T. Jayakumar, and B. Raj, "A defect evaluation methodology based on multiple magnetic flux leakage (MFL) testing signal eigenvalues," *Res. Nondestruct. Eval.*, vol. 27, no. 1, pp. 1–25, 2015.
- [10] D. Wu, S. Lingxin, W. Xiaohong, and L. Zhitian, "A novel non-destructive testing method by measuring the change rate of magnetic flux leakage," *J. Nondestruct. Eval.*, vol. 36, no. 2, p. 24, 2017.
- [11] A. Sophian, G. Y. Tian, and S. Zairi, "Pulsed magnetic flux leakage techniques for crack detection and characterization," *Sens. Actuators A, Phys.*, vol. 125, no. 2, pp. 186–191, 2006.
- [12] T. Zhang, G. Tian, and X. Zuo, "Pulsed magnetic flux leakage sensor systems and applications," in *Proc. Instrum. Meas. Technol. Conf. (I2MTC)*, 2011, pp. 1–6.
- [13] Y. Li, J. Wilson, and G. Y. Tian, "Experiment and simulation study of 3D magnetic field sensing for magnetic flux leakage defect characterisation," *NDT & E Int.*, vol. 40, no. 2, pp. 179–184, Mar. 2007.
- [14] J. W. Wilson and G. Y. Tian, "Pulsed electromagnetic methods for defect detection and characterisation," *NDT & E Int.*, vol. 40, no. 4, pp. 275–283, 2007.
- [15] L. Yang, H. Fong, and Y. Wong, "The application of wavelet transform in magnetic flux leakage test of pipeline," in *Proc. 10th APCNDT*, 2001.
- [16] J. McClellan and T. Parks, "Eigenvalue and eigenvector decomposition of the discrete Fourier transform," *IEEE Trans. Audio Electroacoust.*, vol. AU-20, no. 1, pp. 66–74, Mar. 1972.
- [17] P. G. Wanda and S. Papadimitriou, "Extraction of imperfection features through spectral analysis," U.S. Patent 7231320, Jun. 12, 2007.
- [18] Y. Sun, *The Plural Function and Integral Transformation*. Beijing, China: Machinery Industry Press, 2016.

Erlong Li was born in Guangshui, Hubei, China, in 1989. He received the B.Sc. and M.Sc. degrees from the School of Mechanical Science and Engineering, Huazhong University of Science and Technology, Wuhan, China, in 2012 and 2014, respectively, where he is currently pursuing the Ph.D. degree.

His current research interests include electromagnetic nondestructive technology and instrumentation.

Yihua Kang was born in Hai'an, Jiangsu, China, in 1965. He received the B.Sc., M.Sc., and Ph.D. degrees from the School of Mechanical Science and Engineering, Huazhong University of Science and Technology (HUST), Wuhan, China, in 1987, 1990, and 1993, respectively.

In 1993, he joined HUST as a Post-Doctoral Fellow, where he was an Adjunct Professor in 1995 and a Professor in 1998. His current research interests include nondestructive testing technology and instrumentation.

Jian Tang was born in Lu'an, Anhui, China, in 1993. He received the B.Sc. degree from the School of Manufacturing Science and Engineering, Sichuan University, Chengdu, China, in 2016. He is currently pursuing the Ph.D. degree with the Huazhong University of Science and Technology, Wuhan, China.

His current research interests include electromagnetic nondestructive technology and instrumentation.

Jianbo Wu was born in Sichuan, China, in 1986. He received the B.Sc., M.Sc., and Ph.D. degrees from the School of Mechanical Science and Engineering, Huazhong University of Science and Technology, Wuhan, China, in 2009, 2010, and 2014, respectively.

He is currently a Lecturer with Sichuan University, Chengdu, China. His current research interests include magnetic flux leakage testing and eddy current testing.

Xizi Yan was born in Wuhan, Hubei, China, in 1994. She received the B.Sc. degree from the School of Mechanical Science and Engineering, Wuhan Institute of Technology, Wuhan, China, in 2016, and the M.Sc. degree from Northeastern University, Boston, MA, USA, in 2018.

Her current research interests include robotics mechanics and control and mechatronics.